Regularization of SAR Tomography for 3-D Height Reconstruction in Urban Areas

Hossein Aghababaee, *Member, IEEE*, Giampaolo Ferraioli, *Senior Member, IEEE*, Gilda Schirinzi, *Senior Member, IEEE*, and Vito Pascazio, *Senior Member, IEEE*

***Abstract*—Height reconstruction in urban areas using multibaseline synthetic aperture radar (SAR) images is still a challenging task. Due to the superimposition of scatterers from different elevations in a same resolution cell, the generation of digital elevation model is not straightforward. Classical SAR interferometry cannot be adopted, while standard SAR tomography (TomoSAR) can fail to well identify and separate the scatterers in case that the relative contribution of a scatterer to the others is insignificant. Moreover, irregular and low number of sampling can increase the ambiguity level and introduce artifacts with strong variance from pixel to pixel. Coping with this problem typically requires large number of datasets with proper sampling. In this paper, contextual information is exploited to reduce the ambiguity and resolve the superimposition of the scatterers regardless of their relative power contributions, even in the case of a limited number of images. In particular, the proposed approach, starting from standard spectral estimators, introduces a regularization term to include the *a priori* information about scene height variation in the array processing chain. The reconstruction problem is set as an energy minimization problem that is solved using graph-cut-based optimization algorithms, where the solution of localization is the linkage between optimization of signal energy along direction of arrival and controlling height variation within the neighbors of selected pixel. Details of experimental results in the form of tomographic slices as well as three-dimensional point cloud generation, from simulated and real datasets are included to demonstrate the effectiveness of the proposed reconstruction approach.**

***Index Terms*—Building layover, graph-cut-based regularization, synthetic aperture radar (SAR) tomography.**

I. Introduction

TODAY, the details of buildings and urban infrastructure can be well studied with modern very high-resolution synthetic aperture radar (SAR) imaging systems, where the data with spatial resolution of up to 1 m are available. Such a resolution is very helpful when the spatial scale of the infrastructures is in the range of a few meters. Coherent stacking interferometry (CSI) such as the small baseline subset [1] and persistent scatterer interferometry (PSI) [2] are the main multibaseline (MB) interferometric techniques that have been frequently employed for 3-D urban height mapping [3]–[5]. The former generally is accounted for by a limitation on spatial and temporal baseline and uses multilooking in order to increase the interferometric phase quality. While the latter typically operates at full resolution and on the scatterers that showing a sufficiently high temporal coherence, such as man-made structures. Moreover, techniques, such as SqueeSAR [6], make the use of advantages of CSI and PSI to deal with the distributed scatterer as well. This technique takes the information of the estimated covariance matrix to identify the equivalent permanent scatterers from decorrelating distributed ones. However, all these techniques are mainly limited only to the dominant scatterer in the desired cell; while due to the side-looking geometry of SAR systems, layover (i.e., superposition of scatterers from ground, facade, and roof) is likely to happen in urban areas. Needless to point out that the higher the spatial resolution, the higher the effect of layover. Layover phenomenon represents a severe limitation for several approaches.

In the last decade, SAR tomography (TomoSAR) [7] was the most popular technique able to deal with the layover issue by profiling the scattering distribution. In addition, by the availability of MB fully polarimetric dataset with interferometric condition, the synthesizing performance is increased and the electromagnetic behavior of illuminated objects that presented in a resolution cell but at different height can be described. In other words, polarimetric TomoSAR brings the possibility to estimate not only the reflectivity of scattering distributions, but also the polarimetric scattering mechanism of each scatterer. In [8], the efficiency of fully polarimetric data in the reconstruction of building's tomogram has been assessed and authors showed that polarimetric data may counteract the possible shortcoming of low number of dataset. Hence, in this paper, by taking the advantage of polarimetric MB dataset, we use the polarimetric TomoSAR model to achieve more improved reconstruction from minimal number of acquisitions, i.e., only three tracks.

By today, many techniques borrowed from the theory of spectral estimation, such as beamforming, Capon, multiple signal classification (MUSIC), or singular value decomposition and compressive sensing [9]–[12], have been exploited to profile the elevation reflectivity. An overview of these different focusing methods can be found in [8] and [13]. Uneven and irregular sampling of MB data, which usually is critical in spaceborne data, can impair the quality of reconstruction and make an

Manuscript received June 11, 2018; revised October 10, 2018 and December 8, 2018; accepted December 20, 2018. Date of publication January 21, 2019; date of current version March 4, 2019. This work was supported in part by the University of Naples Parthenope, Italy, within the framework of the "Bando per il sostegno alla ricerca individuale per il triennio 2015–2017." *(Corresponding author: Hossein Aghababaee.)*

The authors are with the Dipartimento di Ingegneria, Università degli Studi di Naples "Parthenope," Naples 80143, Italy (e-mail: aghababaee@uniparthenope.it; giampaolo.ferraioli@uniparthenope.it; gilda.schirinzi@uniparthenope.it; vito.pascazio@uniparthenope.it).

Color versions of one or more of the figures in this paper are available online at http://ieeexplore.ieee.org.

Digital Object Identifier 10.1109/JSTARS.2018.2889428

ambiguous profile for separation of the superimposed scatterers [10]. Moreover, from pixel to pixel, the presence of different artifacts or perturbations of interferometric noise may reduce the accuracy of localization. Generally, the effect of improper sampling, low number of baselines, and decorrelating scatterers is severe in TomoSAR focusing, leading strong worsening in the separation of the superimposed scatterers when the relative power of a scatterer to the dominant one is not perceptible.

To address the problem of accurate estimation of true scatterers, some detection methods, such as generalized-likelihood ratio test (GLRT) [14], support estimation GLRT [15], penalized-likelihood criteria [16], for mitigating the outliers have been employed. These techniques were a kind of single look detectors, which allows preserving full spatial azimuth-range resolution, while the main concern might be the number of detected scatterers in the scene. Moreover, the techniques are limited by numerical complexity that increases with the size of unknown vector, and the detection can be impaired in the area with low SNR. Most recently, the drawback of SNR in the detection process has been mitigated by appropriate multilooking in [17]. At the cost of losing spatial resolution, detection capability over man-made targets as well as in the areas characterized by a low SNR has been improved.

Generally, urban TomoSAR aims at the generation of full 3-D height map of man-made infrastructures. Under the ideal condition (*f.i.* proper baseline sampling, enough number of images, and absence of phase error), and regardless of inversion method, two classes of reconstructed reflectivity can be expected. First, in the case of lower resolution image with *L*- or *P*-band, where a larger number of elementary scatterers are typically presented in a resolution cell, the reflectivity is expected to have strong peaks located in correspondence of the height values of the scatterers. Second, in the case of lower wavelength and point-like scatterers, the profile is superposition of k Dirac delta functions. Hence, by the availability of such profiles, 3-D point cloud generation from superimposed scatterers can be easily performed by peak-finding in the former case and delta location in latter within the obtained tomographic profiles. Along this line, data-adaptive Capon filter [18], MUSIC [19] can achieve a significant height super-resolution capability and sidelobe reduction. However, as mentioned before, under realistic conditions, reconstruction of such a profile is a complicated task. Depart from data acquisition conditions and parameters, the quality of reconstruction methods is dependent to the estimated sample covariance matrix. Traditional way of estimation is a boxcar method that consists in averaging the neighborhood pixels, which may lead to a mix of the information of scatterers belonging to the different objects. Recently, the efficiency of nonlocal SAR (NLSAR) approaches [20] in covariance matrix estimation for 3-D reconstruction of tomographic MB data over mand-made [21] and forested areas [22] has been assessed. The obtained results verified a better reconstruction with nonlocal approaches.

In this paper, we investigate a framework of robust reflectivity profile reconstruction using fully polarimetric data, going through the above-mentioned problems, with the final aim of point cloud generation. To do this, in the first step and in order to prevent from confusion of scatterers from different objects, the covariance matrix is estimated based on the selection of local and NL pixels sharing statistical similarity with the considered pixel.

In the second step and following the idea presented in [23], we use the contextual information as an additional term in the solution of spectral estimation techniques (in particular Capon and MUSIC) to well distinguish the superimposed scatterers and cope with the perturbations of interferometric noise and artifacts. Such a reconstruction allows a tradeoff between the solution of spectral estimations and the height variation within the neighborhood pixels. The latter, commonly named regularization, mitigates the generation of artifacts. The interaction of spectral estimation and regularization can turn to be difficult to be optimized. For this aim, we adopted a graph cut minimization based strategy. A peculiar graph that is able to exploit jointly all the pixels based on the Ishikawa model [24] is built and minimized using a maximum-flow/minimum-cut approach.

A reference to prior works is required in order to assess and highlight the innovative aspects of the proposed approach. Compared to [28], the proposed algorithm introduces the exploitation of the contextual information, and focuses on an urban scenario. In [26], the contextual information is exploited, but for interferometric applications. With respect to the paper presented in [23], the proposed framework exploits a similar methodological approach, but moves forwards, by facing and handling the problem of layover; with reference to [21], the analysis is not limited only on the exploitation of NL approaches for the TomoSAR reconstruction, but the regularization and the optimization steps are introduced and their effects are evaluated. A similar approach to the one proposed in this paper has been recently presented in [25]. The authors propose to regularize the generated point clouds using typical spectral estimation techniques based on geometrical projection and on a peculiar energy minimization. The main limitations of this approach are related to projection steps and to the use of, even if limited, multilook operation. Both issues are not considered in the approach proposed in this paper. Moreover, the presented technique, different from [25], can be easily extended to forest case, making it a useful 3-D height generator also in nonman-made areas. Finally, it is important to highlight that at the best of authors' knowledge, the proposed framework is the first attempt to jointly perform tomographic focusing and spatial regularization directly from the covariance matrix.

This paper is organized as follows. Section II describes the polarimetric tomographic model. The modified polarimetric spectral estimation including regularization term; the nonconvex energy optimization problem is presented in Section III. In Section IV, experimental results obtained on different simulated and real data are shown by pointing out on the main problems of standard focusing and improvement obtained by the proposed model. Finally, conclusions and discussion are drawn in Section V.

II. Polarimetric TomoSAR Model

In this paper, an established signal model of polarimetric MB data from low frequency systems (*L*- and *P*-band) with

N antennas affected by speckle phenomenon as multiplicative noise is considered. Accordingly, MB TomoSAR complex data of each pixel may content one or several distributed targets, and still tomographic stack is a superposition of *L* distributed backscattering mechanisms at different heights. We assume that the stack data are coregistered with respect to a given (master) image, de-ramped and accurately compensated to the phase error. Therefore, the resulting polarimetric MB target vector $\mathbf{x}$, in lexicographic representation can be expressed as [8]

$$\mathbf{x} = \frac{1}{2}\left[\mathbf{x}_{HH}^T \sqrt{2}\mathbf{x}_{HV}^T \mathbf{x}_{VV}^T\right]^T = \sum_{l=1}^{L} \sqrt{\tau_l} s_l \odot \mathbf{b}(z_l) + \mathbf{n} \quad (1)$$

where $\mathbf{x}$ is composed of three MB complex vectors in conventional linear polarizations, $\odot$ represents the Hadamard product, *T* indicates transpose operator, and $\mathbf{n}$ denotes the additive noise. The polarimetric reflectivity and the multiplicative noise vector of source *l* are symbolized by τ_l and $\mathbf{s}_l$; and $\mathbf{b} = [k_1\mathbf{a}(z_l)^T\ k_2\mathbf{a}(z_l)^T\ k_3\mathbf{a}(z_l)^T]^T$ is the polarimetric steering vector, in which $\mathbf{k} = [k_1, k_2, k_3]$ is a unitary reflection mechanism and $\mathbf{k}^{\mathrm{H}}\mathbf{k} = 1$, where *H* denotes the Hermitian. Moreover, $\mathbf{a}(z_i)$ is typical steering vector at height *z* expressed by

$$\mathbf{a}(z_i) = [1, \exp(i2\pi\xi_2 z_i), \exp(i2\pi\xi_3 z_i), \ldots, \exp(i2\pi\xi_n z_i)]^T \quad (2)$$

and $\xi_n = 2b_n/\lambda r$, where the parameters b_n, λ, and *r* indicate orthogonal baselines, wavelength, and range distance, respectively. It should be noted that from physical point of view, the reflectivity τ specifies the backscattering power, which is denoted as SPAN in the polarimetric SAR literatures [27].

The measured MB lexicographic polarimetric vector in (1) has circular Gaussian random distribution with zero mean and covariance matrix of $\mathbf{R}$, given by

$$\mathbf{R} = E\left\{\mathbf{x}\mathbf{x}^H\right\} = \sum_{l}^{L} \tau_l \mathbf{C}_l \odot \mathbf{b}(z_l)\mathbf{b}(z_l)^H + \sigma_n^2\mathbf{I} \quad (3)$$

where $E\{.\}$ is the expectation operator, $\mathbf{C}_l$ is the covariance matrix of multiplicative noise vector $\mathbf{s}_l$, $\mathbf{I}$ is $3N \times 3N$ identity matrix, and σ_n is the standard deviation of adaptive noise.

The estimation of the polarimetric reflectivity can be carried out using different techniques. In this paper, we will focus on two of them: the polarimetric Capon and MUSIC, which are among the most competitive ones [8], [28].

A. Polarimetric Spectral Reconstruction Methods

For the classical polarimetric Capon spectral estimation, a filter is designed to maintain undistorted the signal in directional of arrival while attenuating at all other directions. More precisely, the minimization problem of polarimetric Capon can be represent by [29]

$$\min_h h^H \mathbf{R} h \quad \text{subject to} \quad h^H \mathbf{b}(z,k) = 1 \quad (4)$$

where $\mathbf{b}(z, k) = \mathbf{k}\otimes\mathbf{a}(z)$ is the polarimetric steering vector, $\otimes$ denotes the Kronecker product. It can be proven that the spectrum or polarimetric reflectivity (P_C) from the solution of (4) is represented by [8]

$$P_C(z) = \frac{1}{\lambda_{\min}(\mathbf{b}(z,\mathbf{k})^H \hat{\mathbf{R}}^{-1}\mathbf{b}(z,\mathbf{k}))} \quad (5)$$

where $\lambda_{\min}(.)$ is the minimum eigenvalue operator, and the data covariance matrix $\mathbf{R}$ is substituted by sample covariance matrix $\hat{\mathbf{R}}$ as

$$\hat{\mathbf{R}} = \frac{1}{M}\sum_{m=1}^{M} \mathbf{x}(m)\,\mathbf{x}(m)^H \quad (6)$$

that estimated over *M* independent and identically distributed samples.

Moving to MUSIC, it is an efficient reconstruction technique based on the orthogonality between the steering vector and the noise subspace on its objective function [19]. By refereeing to [8], the spectrum of polarimetric MUSIC can be expressed as

$$P_{Mu}(z) = \frac{1}{\lambda_{\min}(\mathbf{b}(z,\mathbf{k})^H \mathbf{E}_\mathbf{n}\mathbf{E}_\mathbf{n}^H \mathbf{b}(z,\mathbf{k}))} \quad (7)$$

where $\mathbf{E}_\mathbf{n}$ is a noise subspace of the sample covariance matrix using eigenvector decomposition.

Once the polarimetric reflectivity is estimated, the 3-D point cloud can be reconstructed by the retrieved heights of the scatterers for each pixel in (5) or (7).

B. Requirement for Vertical Reflectivity

For the considered distributed model of polarimetric SAR signal in this paper, the reconstructed vertical reflectivity includes peaks correspond to the locations of the *L* superimposed scatterers, which are the solution of layover. Generally, the vertical signal can be described in the terms of resolution, spectral width, and leakage lowering. In TomoSAR focusing, many parameters including residual phase errors, number of acquisitions, and baseline sampling can impair the quality of reconstruction and make difficult or unfeasible to analyze the tomograms of the building layover. From our experiments (see Section III), it is revealed that this is a very severe problem in case that the power contribution of a scatterer to the others is small. In particular, it can usually happen that the ground or roof contribution is missed in the reconstructed vertical profile when their backscattering power is negligible to the facade backscattering. The overall effect of this problem is the presence of a large gap in the point cloud generation of building in ground geometry. Moreover, the presence of strong interferometric phase noise and artifacts in the reconstructed reflectivity profile limits the accuracy in extracting true position of the scatterers.

These two above-mentioned problems make 3-D point cloud generation a nontrivial operation. Consequently, the main required characteristic for the reconstructed reflectivity profile is possession of strong main-lobes in the exact location of *L* scatterers. By taking this specification into account, we seek a possible way to modify the reconstruction of polarimetric spectral estimations in order to identify and separate the scatterers.

III. Regularized Polarimetric TomoSAR

Generally, context is an important source of information in SAR images and many targets need to be recognized in their spatial context. More specifically, in distributed targets, the information relevant to a pixel is strictly related to its surrounding pixels. It is readily understandable that the exploitation of the contextual information provides a kind of regularization that derives from the natural properties of the imaged scene.

Generally, facade can be well reconstructed by standard focusing in (5) or (7), while the main concern is related to the ground and roof's scatterers. To cope with this possible issue, we investigated the use of contextual information (related to ground and roof) in TomoSAR focusing. Following the idea proposed in [23], where the contextual information was used to improve MB phase unwrapping, we consider a framework to combine the solution of polarimetric reconstructions and height variation in the neighborhood pixels. The framework is based on the fact that in urban areas the height is almost constant from pixel to pixel, when the pixels belong to a specific infrastructure, while the height changes suddenly from a pixel to another one, when these two pixels belong to different infrastructures. Accordingly, an *a priori* that controls the height variation between neighborhood pixels could be modeled by [23]

$$\sum_{q} |z - z_q| \tag{8}$$

where q indicates the neighboring pixels of desired one. This term can be used as a contextual information to regularize tomogram and improve the quality of the reconstruction in order to qualify the required characteristic of reflectivity profile. Hence, starting from (5), the modified polarimetric Capon called regularized polarimetric Capon is introduced as

$$P_{RC}(z) = \frac{1}{\lambda_{\min}(\mathbf{b}(z,\mathbf{k})^H \hat{\mathbf{R}}^{-1}\mathbf{b}(z,\mathbf{k})) + \beta \sum_q |z - z_q|}. \tag{9}$$

Using (6) and *a priori* term, the regularized polarimetric MUSIC, in the same way, is given by

$$P_{RMu}(z) = \frac{1}{\lambda_{\min}(\mathbf{b}(z,\mathbf{k})^H \mathbf{E_n}\mathbf{E_n}^H \mathbf{b}(z,\mathbf{k})) + \beta \sum_q |z - z_q|}. \tag{10}$$

In both (9) and (10) β is a parameter that balances relative importance of the two employed terms, and z_q is the height of surrounded pixels.

For the sake of simplicity and without losing the generality, we can assume that only one scatterer exists in the pixels, i.e., $L = 1$. The additive term in the denominator of (9) and (10) gives rise to the heights that are far away from the height of scatterer, and consequently reduce the power of spectrum along these heights, accordingly, leading to side-lobe suppression. However, the main concern of the reconstruction using introduced regularized techniques is related to employment of z_q in (9) and (10) that needs the knowledge of neighborhood pixels' elevation. A proposed strategy to get through this problem is definition of an optimization based on the energy term from the solution of spectral estimation and additive term from contextual information. Such an optimization for each case in (9) and (10) is given as

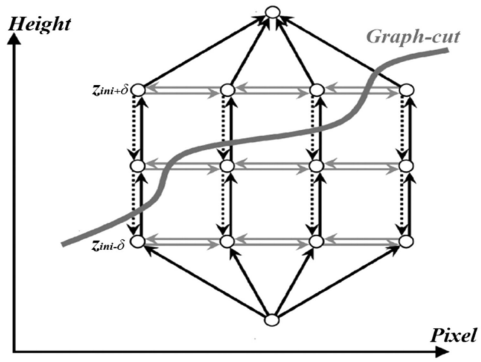

Fig. 1. Graph-cut-based minimization.

For the case of Capon:

$$\hat{z} = \arg\min_{z}\{\lambda_{\min}(\mathbf{b}(z,\mathbf{k})^H \hat{R}^{-1}\mathbf{b}(z,\mathbf{k})) + \beta \sum_q |z - z_q|\}$$

For the case of MUSIC:

$$\hat{z} = \arg\min_{z}\{\lambda_{\min}(\mathbf{b}(z,\mathbf{k})^H \mathbf{E_n}\mathbf{E_n}^H \mathbf{b}(z,\mathbf{k})) + \beta \sum_q |z - z_q|\}. \tag{11}$$

By simultaneity minimization on the height of selected and neighborhood pixels using (11), the solution is the estimated heights for the selected pixel and its connected neighborhoods. The reflectivity may then be reconstructed by inserting the neighborhood heights determined from (11) in the regularized expressions given in (9) and (10).

Simultaneous minimization in (11) turns to be difficult. To this aim a graph cut minimization based strategy [24] is adapted. From the selected pixel and its neighborhood, a graph with L height layers (correspond to the height of ambiguity) can be built (see Fig. 1), where the nodes of the graph are related to the energy terms from spectral estimation techniques at each height layer. From the graph, the solution of (11) is seeking for a graph-cut whose sum of energy term and height variation in all pixels along the graph-cut is minimum between all other possible cuts. Details on the graph construction and the related optimization are given in the following section.

A. Graph Construction and Optimization

To build the graph, the range of height of ambiguity is discretized into L heights layer and then a graph containing nodes is constructed. However, since, typically more than one scatterer exist in each pixel, *f.i.* ground, facade, roof, the minimization in (11) is repeated by building two different graphs around the range of lowest and highest scatterer's elevation (ground and roof) that can be initially estimated by standard TomoSAR in (5) and (7). Both graphs can be constructed in the range of $[z_{\rm ini} - \delta\ z_{\rm ini} + \delta]$, where $z_{\rm ini}$ is the initial height of ground or roof, and δ in our implementation is tuned to $\delta = 5$ m. The resolution step is set to be 0.5 m in the tomogram reconstruction. By performing minimization using these two graphs, two

different contextual information at ground and roof height levels are estimated and then, the regularized polarimetric reconstruction techniques in (9) and (10) are replaced by

$$P_{RC}(z) = \sum_{k=1,2} \frac{0.5}{\lambda_{\min}(\mathbf{b}(z,\mathbf{k})^H \hat{\mathbf{R}}^{-1}\mathbf{b}(z,\mathbf{k})) + \beta \sum_q \left|z - z_q^k\right|}$$

$$P_{RMu}(z) = \sum_{k=1,2} \frac{0.5}{\lambda_{\min}(\mathbf{b}(z,\mathbf{k})^H \mathbf{E_n}\mathbf{E_n}^H \mathbf{b}(z,\mathbf{k})) + \beta \sum_q \left|z - z_q^k\right|} \tag{12}$$

where z_q^1 and z_q^2 are the heights of neighborhood pixels at ground and roof levels, which are obtained from two graphs minimization at their height levels. It should be noted that in our implementations, the neighborhood pixels are selected using four-connected window.

Let us see, in details, how the graph is built. The construction is the same for both graphs (the one related to the ground and the one related to roof). Following the approach of Ishikawa, the graph contains a set of vertexes $v_{i,j}$, two special vertexes (the sink and the tank), and a set of edges *E* [24]. In Fig. 1, the 1-D representation of the graph is shown. Each vertex is identified by two subscripts: *i* which is related to the pixel index, and *j* which is related to the height value (i.e., the labels) that the pixel can assume, within the interval $[z_{\text{ini}} - \delta\ z_{\text{ini}} + \delta]$. The total number of vertexes in the graph will be equal to the number of the considered pixels times the number of possible labels. Concerning the Edges, they are set according to the following values: the vertical ones, $E_{i,j}$ are set to be equal to the first term of (11), computed for the pixel *i* and the label *j*. The horizontal edges, $\mathrm{E}_{i,j+1}$ are set equal to the resolution step (0.5), representing the second term of (11). The algorithm will compute the cut with the minimum cost (sum of the cut edges).

Finding the minimum cut on this particular graph allows obtaining the optimal value for the minimization problem of (11).

B. Implementation Aspects

Regarding the implementation and robust reconstruction some comments are in order. It is obvious that the proposed procedure needs an initial estimation of the covariance matrix. Although the estimation is commonly performed using (6), nonlocal-based approaches, such as NLSAR presented in [20], have proved their effectiveness. Generally, NLSAR is based on the search of nonlocal neighbors of the pixel *t* to be filtered, within a search window of a specific size, that share statistical similarity with the pixel *t* [20]. These similar pixels are then exploited to perform a robust estimation of a covariance matrix. Moreover, controlling over the parameter β is an important issue and necessary for accurate height map generation in an urban area. Its value can be set using the following procedure. At the beginning, β can be set to an initial value equal to the inverse of square root of equivalent number of looks in the estimation of the covariance matrix. In this way, in homogeneous regions many similar neighbors are identified by NLSAR and accordingly number of looks is high, consequently β is set to be a small value, while in nonhomogeneous area with larger value of β, more importance is imposed on the additive term in reflectivity profile reconstruction. After, a refinement of the solution can be obtained by changing the β parameter by trial and error, slightly moving from the initial value. Analysis on the choice of β are reported in Section IV.

Furthermore, it should be noted that the framework can easily be extended to the other techniques of fully polarimetric and also single polarimetric reconstructions in order to improve the quality of reconstruction. To this aim, the defined first energy term in (11) should be changed by the function of employed techniques.

Moreover, the efficiency of the proposed method on the improvement of two-component reflectivity profile of forested area is expected, while the method may not be adapted to the case of a multilayer forest. By considering the two-layer random volume over ground model in forested area, the reconstructed vertical profile is expected to have two phase centers in the position of ground and canopy locations. Accordingly, again in a similar way, two graphs at a ground and canopy height level can be constructed in order to perform the minimization that is required in the regularized reconstruction.

Finally, the reconstruction algorithm can be summarized as

Regularized polarimetric reconstruction framework:
For each pixel
1. Estimate covariance matrix by NLSAR approach.
2. Estimated initial locations of lowest and highest scatterers by standard focusing in (5) or (7)
3. Build two graphs around the range of the lowest and highest scatterers.
4. Perform minimization in (11) for each case and for the constructed graphs and derive the heights of neighborhood pixels.
5. Refine tomogram by (12) for each reconstruction technique

IV. Experimental Results

A. Simulated Data

The proposed framework is, first, evaluated under controlled conditions by using simulated dual baseline fully polarimetric dataset from two different buildings (see Fig. 2). Building A of Fig. 2(a) has a simple structure with flat 35 m height roof, oriented to the radar line of sight (LOS). Building B of Fig. 2(b) is perpendicular to the LOS with an open gable roof, and a height of 28 m in the middle part and 20 m at the beginning. It has been assumed that the ground is covered by small vegetation, and its backscattering is a combination of odd-bounce and volumetric scattering. The backscattering mechanisms from the walls toward LOS is set to the double-bounce and of the roof to the surface or odd-bounce scattering mechanism. The backscattering 3-D points with a specified backscattering mechanism according to [30] and corresponding to the structure of buildings are generated in radar geometry. In the simulation process, in order to meet realistic conditions, power contribution of double bounce is set to be larger than the odd bounce from ground and roof, while their relative power ratio is varying from pixel to pixel. The acquisition parameters are set to the typical values of

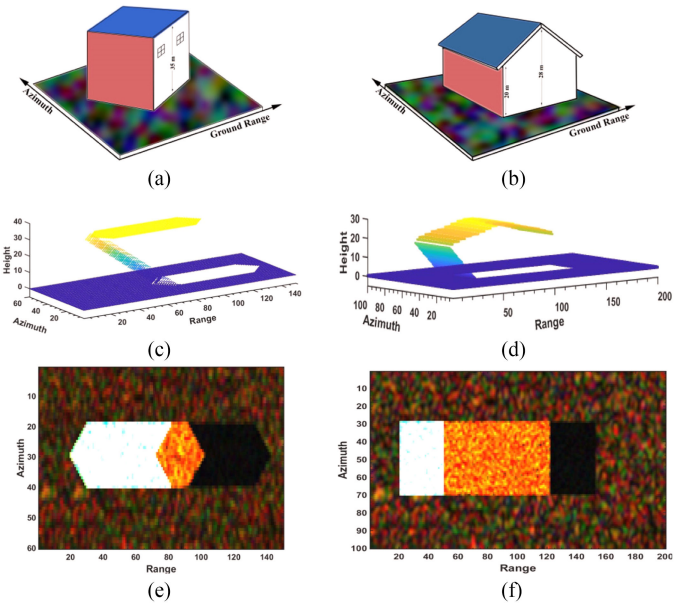

Fig. 2. Simulated scene, (a) and (b) related to Building A and B. Discretized 3-D points from (c) Building A and (d) Building B; Pauli color composite of master images in (e) scene A and (f) scene B.

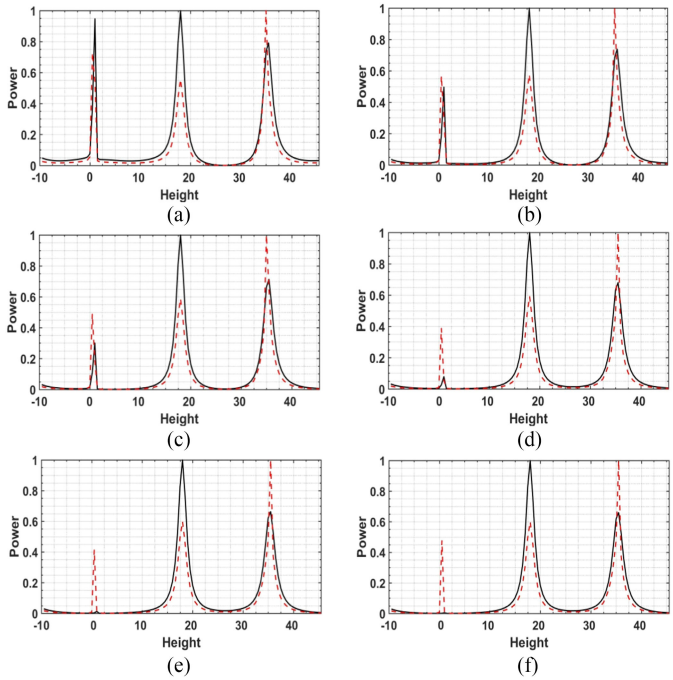

Fig. 3. Reconstructed height profiles for a layovered cell with different relative power contributions. Black and red dash profiles are produced by standard and regularized Capon, respectively. (a) $\sigma_{dbl}/\sigma_{\text{odd}} = 1$. (b) $\sigma_{dbl}/\sigma_{\text{odd}} = 1.2$. (c) $\sigma_{dbl}/\sigma_{\text{odd}} = 1.4$. (d) $\sigma_{dbl}/\sigma_{\text{odd}} = 2.25$. (e) $\sigma_{dbl}/\sigma_{\text{odd}} = 3.35$. (f) $\sigma_{dbl}/\sigma_{\text{odd}} = 4.5$.

airborne *L*-band data in Dresden 2000 by the E-SAR sensor of the DLR [8], with incident angle of 35° , 3550 m flight height, and orthogonal baseline are 10 and 35 m. For each pixel, the steering vector according to the acquisition geometry and the point position is computed, and then polarimetric single look complex images are generated by coherent combination of scatterers through the tomographic (1). Fig. 2(c) and (d) shows the 3-D position of the scatterers in SAR (azimuth, slant range) geometry. Moreover, master images in Pauli color coded are shown in Fig. 2(e) and (f).

The main issue of standard SAR tomography related to layover area is first investigated. An analysis on the behavior of the proposed algorithm with respect to power ration of scatterers is carried out. In the analysis, the layover part of scene A, of Fig. 2, is simulated with different power contribution from facade to the ground and roof. In other words, three scatterers at heights of 0, 18, and 35 m are superimposed. Then, we analyzed the quality of reconstruction when the ratio of power of double bounce to the odd bounce scattering $(\sigma_{dbl}/\sigma_{\text{odd}})$ is increased from 1 to 4.5. The estimated normalized reflectivity profiles from standard Capon and regularized Capon are computed and illustrated in Fig. 3. When these three scatterers have similar power contributions, $(\sigma_{dbl}/\sigma_{\text{odd}} = 1)$ both employed techniques [standard Capon (5) and regularized Capon (12)] are able to distinguish the superimposed scatterers and properly localize the scatterers [see Fig. 3(a)]. However, when the power ratio is increasing, reconstruction of ground contribution from standard Capon is getting complicated, such that with a power ratio of 4.5, ground contribution totally is missed in the reconstructed profile by standard Capon. Instead, the proposed method, by taking the advantage of contextual information from neighborhood pixels (could be some pixels even outside of layovered area), is able to reconstruct the ground regardless of the variation of power contribution. Generally, in urban area, the scatterers with different backscattering power are superimposed. Proper identification of their reflectivity profile needs the high number of MB dataset. However, it can be seen that the contextual information brings the possibility to resolve this shortcoming although with a limited number of images.

In the next experiments, the effect of regularization is analyzed using both employed reconstruction techniques. Frist, we present the tomogram slices obtained from both simulated datasets in a mid-azimuth transect line, and then the implementation is extended to all lines in order to generate 3-D point cloud from the scenes. Fig. 4 shows the true simulated SPAN tomogram and estimated ones from standard and regularized Capon and MUSIC as well. Tomograms are depicted in height-range plane and those have been normalized, such that the maximum along the height for each cell is unitary. In particular, the reconstruction has been done using standard Capon [see Fig. 4(b) and (g)], standard MUSIC [see Fig. 4(c) and (h)], regularized Capon [see Fig. 4(d) and (i)], and regularized MUSIC [see Fig. 4(e) and (j)]. In both datasets, the results obtained from reconstruction techniques (before and after regularization) are very similar in nonlayover areas (ground and only roof), while in layovered areas where there is a superimposition of scatterers from ground, facade and roof, standard Capon based and MUSIC-based reconstruction in (5) and (7) failed to well identify the ground and roof backscattering. This happens because their power contributions are much lower than the double-bounce backscattering from facade, and then reconstruction is unable to well identify the scatterers with a lower power contribution. However, moving to regularized Capon and MUSIC (12), the capability of the

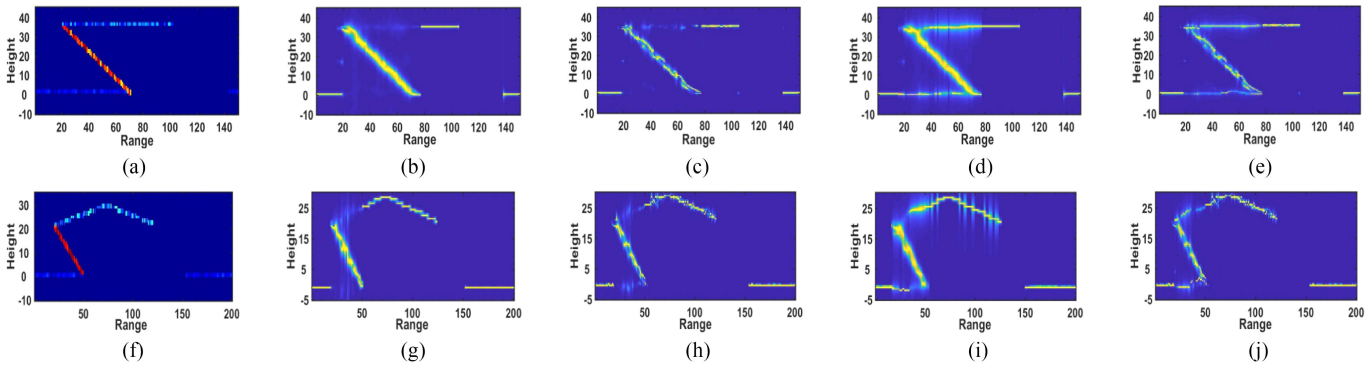

Fig. 4. Tomograms of simulated scenes. (a) and (f) True simulated SPAN tomograms for scene A and B. (b) and (g) Tomograms using standard Capon. (c) and (h) Tomogram using standard MUSIC. (d) and (i) Using regularized Capon. (e) and (j) Tomogram using regularized MUSIC.

TABLE I
RUNNING TIME OF THE IMPLEMENTED METHODS (SECOND)

	Scene A	Scene B
Standard Capon	4.7	6.8
Standard MUSIC	7.8	12.3
Regularized Capon	32.7	44.5
Regularized MUSIC	37.8	52.6

proposed framework in overcoming this drawback by taking the advantage of contextual information is evident. By comparing the two employed reconstruction techniques, as can be expected, MUSIC shows the super-resolution capability and diminished or somehow suppressed the leakages, specifically in regularized ones.

However, it should be pointed out that the improvement by regularization obtained at the cost of processing time. Efficiency of the algorithms with respect to the processing time for the reconstructed tomograms in Fig. 4 is evaluated on a desktop PC with a 7-core processor and presented in Table I. The total running time for regularized Capon and MUSIC is around five times more than standard ones. Although this increasement in the running time can limit the application of proposed framework in TomoSAR processing of large volume dataset, but some tips can be considered in order to reduce the processing time. For example, instead of adapting moving window and performing minimization in (11) for each pixel separately, one can consider a homogeneous patch of image and perform minimization for the current patch. Then easily the height information of all pixels inside the patch is available and can be used for the profile reconstruction in (12).

Another point on the proposed framework is related to the effect of parameter β on the reconstruction performance. In (12), obviously when β is zeros, the reconstructed profile is coincident to the standard frameworks, while by increasing the value of this parameter some differences can be expected. Fig. 5 shows the reconstructed profiles from standard and regularized Capon for a simulated layover scenario with three scatterers. For the large value of β, the standard deviation of estimated heights in moving window is small, and generally all pixels inside the window have similar or same heights. Accordingly, the reflectivity profile gives strong raise in the corresponding

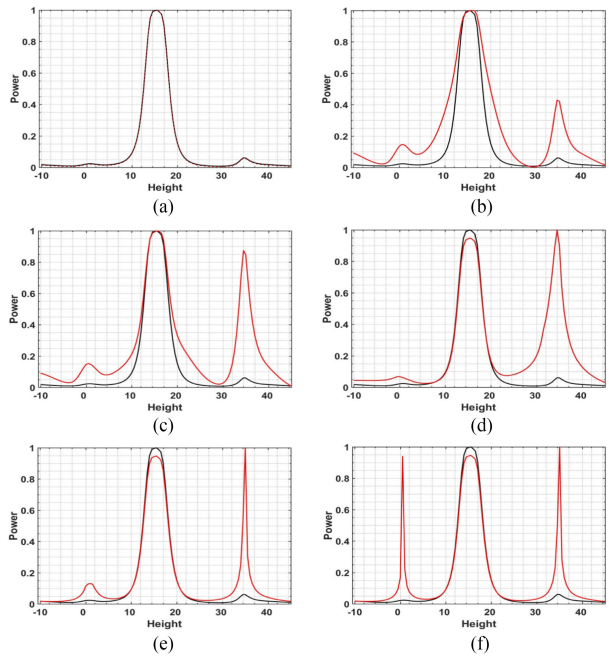

Fig. 5. Effect of parameter β on the reconstruction using proposed framework. Black and red profiles are produced by standard and regularized Capon, respectively. (a) $\beta = 0$. (b) $\beta = 0.01$. (c) $\beta = 0.05$. (d) $\beta = 0.1$. (e) $\beta = 0.35$. (f) $\beta = 0.85$.

height location (see Fig. 5). In the case of small value of β, the standard deviation of estimated height of neighborhood pixels is large, and mild rise in the location of mean of the heights can be expected in the reflectivity profile, where by multiplying it in the small value of β, its effect can even be diminished. Moreover, it should be noted that very large value of β cancels the contribution of middle scatterer.

As stated in the previous section, the optimal value of β is estimated by trial and error starting from an initial value set to the inverse of square root of number of looks. It should be noted that experiments on behaviors of β using regularized MUSIC (not reported here for the sake of conciseness) has similar results shown in Fig. 5.

Furthermore, in Fig. 6, the reconstructed 3-D point clouds from employed techniques are shown. From a 3-D view of the

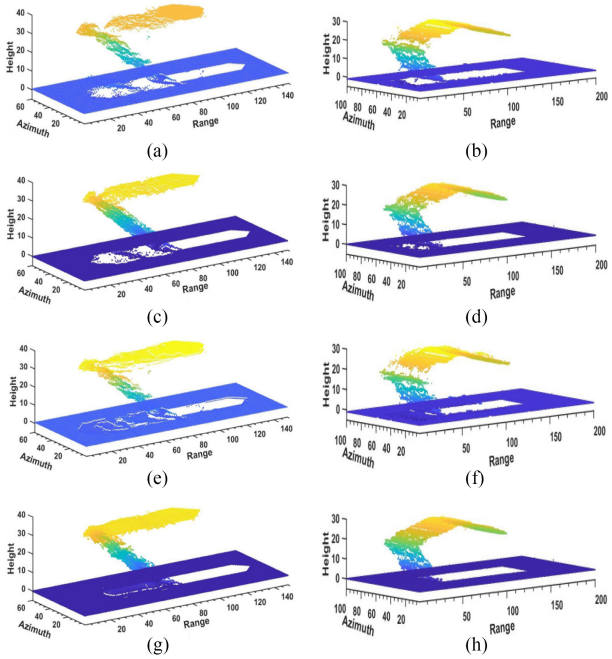

Fig. 6. Point cloud reconstruction from simulated data. (a) Standard Capon. (b) Standard Capon. (c) Standard MUSIC. (d) Standard MUSIC. (e) Regularized Capon. (f) Regularized Capon. (g) Regularized MUSIC. (h) Regularized MUSIC.

TABLE II
SIMULATED DATA A—QUANTITATIVE COMPARISON OF ESTIMATED HEIGHT ERROR (UNIT IS METER)

		Ground	Roof
		$\mu \pm \sigma$	$\mu \pm \sigma$
Layover	Standard Capon	3.80±3.44	1.53±2.51
	Standard Music	3.03±3.41	0.49±0.69
	Regularized Capon	0.48±0.82	0.86±1.94
	Regularized Music	0.37±0.82	0.14±0.31
Whole of the scene	Standard Capon	0.57±1.87	1.2±2.2
	Standard Music	0.34±1.46	0.57±0.77
	Regularized Capon	0.09±0.42	0.75±1.6
	Regularized Music	0.07±0.41	0.25±0.32

TABLE III
SIMULATED DATA B—QUANTITATIVE COMPARISON OF ESTIMATED HEIGHT ERROR (UNIT IS METER)

		Ground	Roof
		$\mu \pm \sigma$	$\mu \pm \sigma$
Layover	Standard Capon	8.36±6.55	2.35±4.18
	Standard Music	5.85±6.00	2.19±3.35
	Regularized Capon	0.60±0.89	1.85±1.49
	Regularized Music	0.46±1.89	0.81±1.37
Whole of the scene	Standard Capon	0.77±3.30	1.02±2.45
	Standard Music	0.46±2.35	0.97±1.53
	Regularized Capon	0.06+0.34	0.86±1.08
	Regularized Music	0.04±0.76	0.69±0.63

TABLE IV
SIMULATED DATA A—QUANTITATIVE COMPARISON OF HEIGHT ESTIMATION (UNIT IS METER)

	Accuracy	Completness
	$\mu \pm \sigma$	$\mu \pm \sigma$
Standard Capon	2.09±6.80	1.61±4.54
Standard Music	1.65±6.32	1.15±4.45
Regularized Capon	1.77±6.21	0.63±1.30
Regularized Music	1.54±6.30	0.22±0.81

TABLE V
SIMULATED DATA B—QUANTITATIVE COMPARISON OF HEIGHT ESTIMATION (UNIT IS METER)

	Accuracy	Completness
	$\mu \pm \sigma$	$\mu \pm \sigma$
Standard Capon	1.35±3.36	1.37±2.53
Standard Music	1.13±4.54	0.77±2.99
Regularized Capon	1.18±2.53	1.11±1.80
Regularized Music	1.01±4.30	0.22±1.32

generated point clouds, it is possible to affirm that the both regularized Capon and MUSIC are more efficient in well detecting the backscattering from ground, roof, and facade. In fact, gap filling in layover area, which is the main limitation of point cloud generation using standard SAR tomography techniques, has been properly addressed in the proposed techniques. The framework strengths the potential of SAR tomography in decomposing the superimposed scatterers by taking into account the contextual information.

In order to quantitatively evaluate the performances of the employed methods, average absolute error μ, and standard deviation σ of the estimated ground and building heights in comparison with the actual ones, are computed and presented in Tables II and III. To highlight the potential of the proposed framework compared to the existing standard reconstruction, evaluation is performed in the layovered area and also across the whole scene. As it can be seen, the layover causes high ground and roof height estimation error when the standard TomoSAR techniques are used for point cloud generation, while, from the quantitative comparisons in the layover regions, the regularized TomoSAR techniques outperform the standard methods and effectively address the problem of decomposing scatterers by correctly estimating their relative heights. In this case, the average error in ground and roof height estimation is significantly decreased (see Tables II and III).

Furthermore, the evaluation of generated point clouds is performed using two measures defined in [21], called accuracy and completeness. Accuracy measures how close the estimated point cloud is to the ground truth and completeness measures how the ground truth is modeled by the estimated points. It should note that these measures are performed independently for each pixel. Tables IV and V show the results of evaluation, where both accuracy and completeness affirm that the results of regularized TomoSAR outperform the standard TomoSAR. Moreover, from the tables, it can be verified that the actual 3-D height model of infrastructures in both datasets is appropriately modeled by small value of completeness, which gives promising way to a 3-D height model of urban area using TomoSAR approaches.

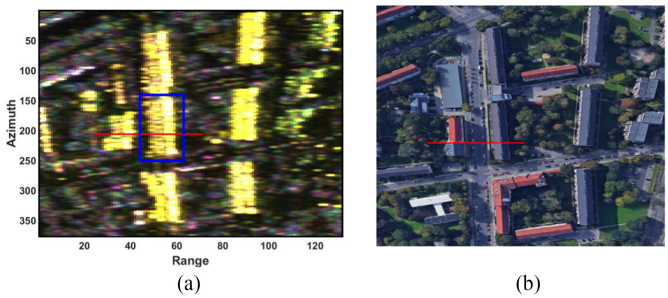

Fig. 7. Real dataset. (a) Pauli color composite of master image. (b) Optical image of study area (courtesy: Google earth).

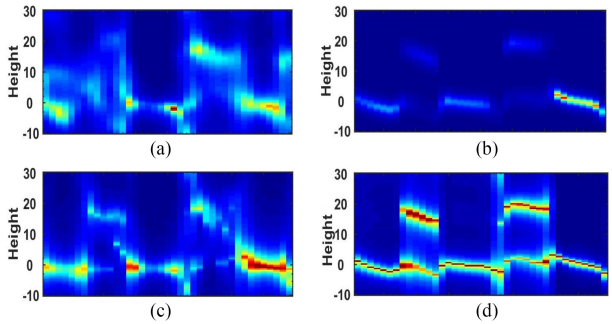

Fig. 8. Tomograms of the transect line, when covariance matrix is estimated using boxcar approach. Horizontal axis of the images is the range direction. (a) Standard Capon. (b) Standard MUSIC. (c) Regularized Capon. (d) Regularized MUSIC.

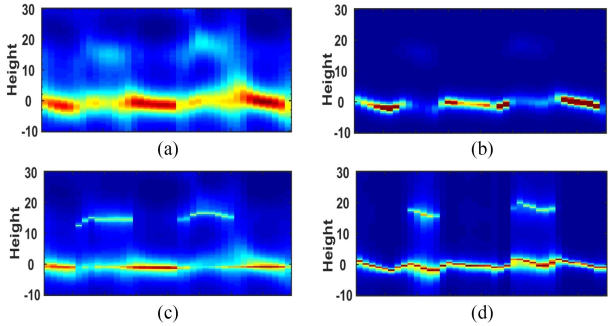

Fig. 9. Tomograms of the transect line, when covariance matrix is estimated using NLSAR approach. Horizontal axis of the images is the range direction. (a) Standard Capon. (b) Standard MUSIC. (c) Regularized Capon. (d) Regularized MUSIC.

B. Real Data

To validate the proposed method, the experiments have been extended to real airborne data. In particular, E-SAR *L*-band (1.3-GHz center frequency) full polarimetric dual-baseline data over the city of Dresden in Germany, acquired on August 1, 2000, have been processed. The Pauli RGB image and the optical images of the study area are shown in Fig. 7. The polarimetric image spatial resolutions are 3.0 m in azimuth and 2.2 m in range direction. With such a resolution, where the presence of a sufficient number of scatterers is covered, the assumption of distributed model is reasonable. The baseline configuration is nonuniform, spanning from 10 m to about 40 m. Incidence angle changes from 25° to 55° from near to far range, while slant range distance varies from 3741.70 to 5892.10 m. With the MB configuration, the height of ambiguity is around 20 m and 98 m in near and far range, respectively. Furthermore, the height Fourier resolution is approximately 15 m in midrange [8].

In analogy to simulated experiments, the analysis of reconstruction using standard and regularized Capon and MUSIC is proceeded. Furthermore, the effect of covariance matrix estimation by using NLSAR and boxcar is studied with the reconstruction of tomographic slice along an azimuth line (indicated with the red line in Fig. 7). Here, it has been studied how contextual information and accurate estimation of covariance matrix can go over through the problems of typical reconstruction. Along the considered transect line two buildings are presented. Both buildings are made up of four floors and a gable roof. Unfortunately, a precise ground truth height for the buildings are not available. The only information on the considered buildings is provided by Google earth. According to it, the height of the buildings are around 16 and 17 m, for the first building (in near range) and the second one, respectively. For the selected line, and after performing de-ramping and proper phase calibration, the tomograms are computed by standard and regularized techniques, with covariance matrix estimated by boxcar and NLSAR. The results are shown in Figs. 8 and 9. Typically, reconstruction by dual baseline data and uneven sampling is a critical task and the tomogram can be affected by high level of ambiguity and artifacts. This can be verified from the reconstructed tomogram by standard Capon and MUSIC with boxcar-based covariance matrix estimation [see Fig. 8(a) and (b)]. This is evident specifically with Capon, where scatterers in the layovered areas are not well identified. From the results, standard Capon failed to reconstruct the ground and roof, specifically for first building, while standard MUSIC produces more focused tomogram. However, still ground scatterers are not recognized in the layovered areas. Regularization of boxcar-based reconstruction from employed techniques are also presented in Fig. 8(c) and (d). From the comparison, it can be verified that, first, the contributions of scatterers on the roof are highlighted by regularized Capon, which were nearly lost in the standard-based Capon. In the same way, regularized MUSIC also gives solution to the ground contribution in layover area, which was missed in the standard one. Second, resolution is enhanced with suppression of sidelobes in the tomograms. However, still some artifacts due to the high ambiguity level of dataset can be observed even after regularization using both methods. In order to improve the quality of tomograms, the NLSAR-based reconstructions are preceded and the results of both cases (before and after regularization) are shown in Fig. 9. By visual comparison, once again the super-resolution capability of MUSIC to the Capon can be verified. Moreover, by comparing results with the obtained results from boxcar-based reconstruction, it can be observed that NLSAR helps to achieve more reliable tomograms by well identification of scatterers. Moreover, it can be seen that building roof's contribution is more emphasized after regularization, which makes it easy to measure infrastructure heights. To sum up, it is possible to affirm from the presented tomograms that the proposed framework (NLSAR and regularization together) exhibits good performance by focusing the backscattering in right heights and overthrow the artifacts, specifically for ground backscatters.

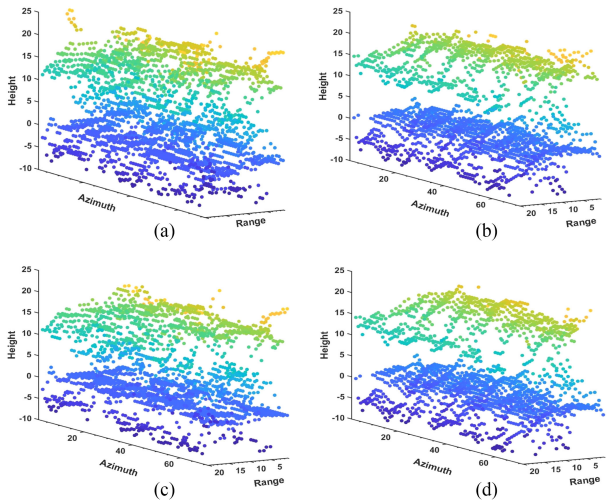

Fig. 10. 3-D view on generated point cloud for area of interest in Fig. 7. The covariance matrix is estimated using boxcar approach. (a) Standard Capon. (b) Standard MUSIC. (c) Regularized Capon. (d) Regularized MUSIC.

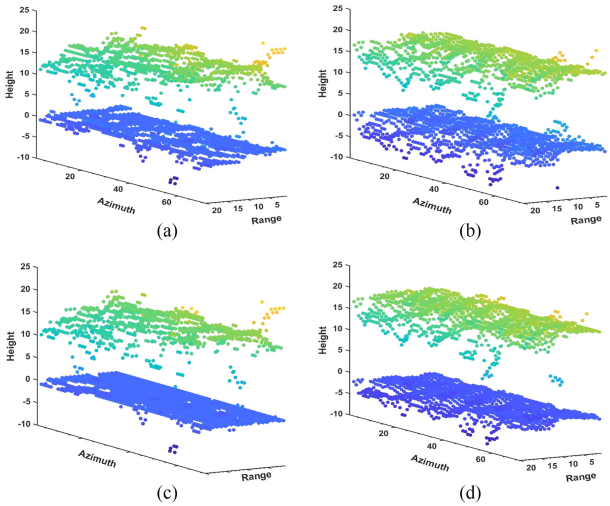

Fig. 11. 3-D view on generated point cloud for area of interest in Fig. 7. The covariance matrix is estimated using NLSAR approach. (a) Standard Capon. (b) Standard MUSIC. (c) Regularized Capon. (d) Regularized MUSIC.

After having employed tomograms, to assess the method in 3-D point cloud generation, the processing chain has been extended to the whole pixels belonging to the second building, indicated by the blue rectangle in Fig. 7(a). Similar to the simulated case, the point cloud is computed by peaks finding in the reconstructed reflectivity profiles. In order to avoid sidelobe detection as a scatterer, main lobes are separated by a simple thresholding on the reflectivity profiles. The effect of regularization and the robust covariance matrix estimation is shown in Figs. 10 and 11 by the generated point clouds. In Fig. 10, the covariance matrix is estimated using a boxcar approach. It can be seen that results by boxcar are strongly affected by outliers; howbeit, regularization reduces this effect [see Fig. 10(c)]. In comparison, MUSIC-based reconstructions are less affected by outliers and ambiguity of data. Nevertheless, in all results presented in Fig. 10, some unresolved layover, undetected ground or roof scatterers can be observed. Generally, results of regularization after estimation of covariance matrix by boxcar are

TABLE VI
QUANTITATIVE COMPARISON OF THE GROUND SCATTERERS HEIGHT (UNIT IS METER)

	Boxcar	NLSAR
	$\mu \pm \sigma$	$\mu \pm \sigma$
Standard Capon	-0.80±3.74	-0.85±1.21
Standard MUSIC	-1.48±3.03	-1.19±1.95
Regularized Capon	-0.78±3.50	-1.00±0.91
Regularized MUSIC	-1.06±3.03	-0.46±1.61

TABLE VII
QUANTITATIVE COMPARISON OF THE ROOF SCATTERERS HEIGHT (UNIT IS METER)

	Boxcar	NLSAR
	$\mu \pm \sigma$	$\mu \pm \sigma$
Standard Capon	17.20±5.22	15.76±3.78
Standard MUSIC	17.86±5.18	17.19 ±3.79
Regularized Capon	16.61±4.90	15.36±3.77
Regularized MUSIC	15.78±3.74	15.84±3.63

still affected by some outliers and unresolved superimposed scatterers, which stressing the role of covariance matrix inside the energy term are defined by standard Capon and MUSIC equations. Using the NLSAR approach for covariance matrix estimation (see Fig. 11) strongly reduces the outliers. In this case, in the results by standard reconstruction techniques, some undetected ground or roof scatterers are evident, while the employed regularized Capon and MUSIC with NLSAR effectively resolve the layover issue. From the results, employment of NLSAR and regularization together can verify the ability of the proposed framework in well identifying the structures of building using MB SAR dataset. As mentioned before, the height of the analyzed building is in the range of 16–17 m, while the ground scatterers have zero elevation. Accordingly, quantitative analysis can be performed by assessing the standard deviation of height variation of ground and roof scatterers in the generated point clouds. In the point cloud, all the scatterers with height of less than 5 m and more than 10 m are considered as ground and roof scatterers, respectively. By this assumption, Tables VI and VII represent the mean and standard deviation of height variations. From the tables, it can be affirmed that the height variations in all cases are limited by the regularized TomoSAR with respect to the standard one, which are more fitted to the actual building's height.

V. CONCLUSION

This paper focuses on the main limitations of SAR tomography in urban area for proper reconstruction of reflectivity profile with final aim of point cloud generation. Two main limitations strongly affect the reconstruction from standard array processing techniques and make in somehow unfeasible and complicated resolving the superimposed scatterers in height directions. The first one is related to the low number of datasets, while the second is the unequal relative power ratio of the scatterer. To mitigate the effect of these problems, we proposed a framework that employs contextual information as an additive term in the reconstruction from array processing techniques. In particular,

the contextual information is added to the standard polarimetric Capon and MUSIC methods. This term controls the height variation within the neighborhood of selected pixel. The focusing can be seen as a minimization problem, effectively solved using a graph-cut-based optimization algorithm.

The proposed framework has been implemented and evaluated on both simulated and real dataset with minimal number of acquisitions, i.e., only three tracks. The simulated data test was tailored to analyze the separation of super-imposed scatterers from ground, facade, and roof, with more power contribution from the facade. Performance analysis showed that in both cases the regularized techniques outperform the standard spectral estimations in both quality of reconstruction by addressing layover and gap filling in 3-D point cloud generation. Moreover, results from a real dataset showed that the employment of contextual information can mitigate the ambiguity level in focusing due to the low number of MB dataset and uneven baseline sampling. The importance of the covariance matrix estimation is the reconstruction that has been stressed out by comparing the obtained tomograms based on boxcar and NLSAR methods. NLSAR estimation of a covariance matrix led to mitigate the artifact effect issued by standard reconstruction techniques, while the joint use of a regularized method and NLSAR allows the overcoming of the aforementioned problems. The use of a graph-cut-based approach guarantees to obtain an optimal solution for the estimation problem. The obtained improvements by regularization are paid in somehow at the cost of computational efforts. Thanks to the use of the graph-cut-based approach, the algorithm and its implementation are easy and fast, but still more time consuming than standard focusing. It is worth noting that the proposed method in a general framework can extend to the other techniques of fully and single polarimetric reconstructions or using a combination of them. Moreover, the benefits of the proposed approach on the forest structure retrieval could be addressed and analyzed in future works.

ACKNOWLEDGEMENT

The authors wish to thank the German Aerospace Center (DLR) for supplying the E-SAR data.

REFERENCES

[1] P. Berardino, G. Fornaro, R. Lanari, and E. Sansosti, "A new algorithm for surface deformation monitoring based on small baseline differential SAR interferograms," *IEEE Trans. Geosci. Remote Sens.*, vol. 40, no. 11, pp. 2375–2383, Nov. 2002.

[2] A. Ferretti, C. Prati, and F. Rocca, "Nonlinear subsidence rate estimation using permanent scatterers in differential SAR interferometry," *IEEE Trans. Geosci. Remote Sens.*, vol. 38, no. 5, pp. 2202–2212, Sep. 2000.

[3] F. Baselice, A. Budillon, G. Ferraioli, V. Pascazio, and G. Schirinzi, "Multibaseline SAR interferometry from complex data," *IEEE J. Sel. Topics Appl. Earth Observ. Remote Sens.*, vol. 7, no. 7, pp. 2911–2918, Jul. 2014.

[4] M. Crosetto, O. Monserrat, M. Cuevas-González, N. Devanthéry, and B. Crippa, "Persistent scatterer interferometry: A review," *ISPRS J. Photogrammetry Remote Sens.*, vol. 115, pp. 78–89, 2016.

[5] G. Fornaro, A. Pauciullo, and F. Serafino, "Deformation monitoring over large areas with multipass differential SAR interferometry: A new approach based on the use of spatial differences," *Int. J. Remote Sens.*, vol. 30, no. 6, pp. 1455–1478, 2009.

[6] A. Ferretti, A. Fumagalli, F. Novali, C. Prati, F. Rocca, and A. Rucci, "A new algorithm for processing interferometric data-stacks: SqueeSAR," *IEEE Trans. Geosci. Remote Sens.*, vol. 49, no. 9, pp. 3460–3470, Sep. 2011.

[7] A. Reigber and A. Moreira, "First demonstration of airborne SAR tomography using multibaseline L-band data," *IEEE Trans. Geosci. Remote Sens.*, vol. 38, no. 5, pp. 2142–2152, Sep. 2000.

[8] S. Sauer, L. Ferro-Famil, A. Reigber, and E. Pottier, "Three-dimensional imaging and scattering mechanism estimation over urban scenes using dual-baseline polarimetric InSAR observations at L-Band," *IEEE Trans. Geosci. Remote Sens.*, vol. 49, no. 11, pp. 4616–4629, Nov. 2011.

[9] A. Budillon, A. Evangelista, and G. Schirinzi, "Three-dimensional SAR focusing from multipass signals using compressive sampling," *IEEE Trans. Geosci. Remote Sens.*, vol. 49, no. 1, pp. 488–499, Jan. 2011.

[10] G. Fornaro, F. Lombardini, and F. Serafino, "Three-dimensional multipass SAR focusing: Experiments with long-term spaceborne data," *IEEE Trans. Geosci. Remote Sens.*, vol. 43, no. 4, pp. 702–714, Apr. 2005.

[11] F. Gini, F. Lombardini, and M. Montanari, "Layover solution in multibaseline SAR interferometry," *IEEE Trans. Aerosp. Electron. Syst.*, vol. 38, no. 4, pp. 1344–1356, Oct. 2002.

[12] X. X. Zhu and R. Bamler, "Tomographic SAR inversion by norm regularization;the compressive sensing approach," *IEEE Trans. Geosci. Remote Sens.*, vol. 48, no. 10, pp. 3839–3846, Oct. 2010.

[13] G. Fornaro, F. Lombardini, A. Pauciullo, D. Reale, and F. Viviani, "Tomographic Processing of Interferometric SAR Data: Developments, applications, and future research perspectives," *IEEE Signal Process. Mag.*, vol. 31, no. 4, pp. 41–50, Jul. 2014.

[14] A. Pauciullo, D. Reale, A. D. Maio, and G. Fornaro, "Detection of double scatterers in SAR tomography," *IEEE Trans. Geosci. Remote Sens.*, vol. 50, no. 9, pp. 3567–3586, Sep. 2012.

[15] A. Budillon and G. Schirinzi, "GLRT based on support estimation for multiple scatterers detection in SAR tomography," *IEEE J. Sel. Topics Appl. Earth Observ. Remote Sens.*, vol. 9, no. 3, pp. 1086–1094, Mar. 2016, doi: 10.1109/JSTARS.2015.2494376.

[16] X. X. Zhu and R. Bamler, "Super-resolution power and robustness of compressive sensing for spectral estimation with application to spaceborne tomographic SAR," *IEEE Trans. Geosci. Remote Sens.*, vol. 50, no. 1, pp. 247–258, Jan. 2012.

[17] A. Pauciullo, D. Reale, W. Franzé, and G. Fornaro, "Multi-look in GLRT-based detection of single and double persistent scatterers," *IEEE Trans. Geosci. Remote Sens.*, vol. 56, no. 9, pp. 5125–5137, Sep. 2018.

[18] J. Capon, "High-resolution frequency-wavenumber spectrum analysis," *Proc. IEEE*, vol. 57, no. 8, pp. 1408–1418, Aug. 1969.

[19] R. Schmidt, "Multiple emitter location and signal parameter estimation," *IEEE Trans. Antennas Propag.*, vol. AP-34, no. 3, pp. 276–280, Mar. 1986.

[20] C. A. Deledalle, L. Denis, F. Tupin, A. Reigber, and M. Jäger, "NL-SAR: A unified nonlocal framework for resolution-preserving (Pol)(In)SAR denoising," *IEEE Trans. Geosci. Remote Sens.*, vol. 53, no. 4, pp. 2021–2038, Apr. 2015.

[21] O. D'Hondt, C. López-Martínez, S. Guillaso, and O. Hellwich, "Nonlocal filtering applied to 3-D reconstruction of tomographic SAR data," *IEEE Trans. Geosci. Remote Sens.*, vol. 56, no. 1, pp. 272–285, Jan. 2018.

[22] H. Aghababaee, G. Ferraioli, G. Schirinzi, and M. R. Sahebi, "The role of nonlocal estimation in SAR tomographic imaging of volumetric media," *IEEE Trans. Geosci. Remote Sens. Lett.*, vol. 15, no. 5, pp. 729–733, May 2018.

[23] G. Ferraioli, C. A. Deledalle, L. Denis, and F. Tupin, "Parisar: Patch-based estimation and regularized inversion for multibaseline SAR interferometry," *IEEE Trans. Geosci. Remote Sens.*, vol. 56, no. 3, pp. 1626–1636, Mar. 2018.

[24] H. Ishikawa, "Exact optimization for Markov random fields with convex priors," *IEEE Trans. Pattern Anal. Mach. Intell.*, vol. 25, no. 10, pp. 1333–1336, Oct. 2003.

[25] A. Ley, O. D'Hondt, and O. Hellwich, "Regularization and completion of TomoSAR point clouds in a projected height map domain," *IEEE J. Sel. Topics Appl. Earth Observ. Remote Sens.*, vol. 11, no. 6, pp. 2104–2114, Jun. 2018.

[26] J. Kang, Y. Wang, M. Körner, and X. X. Zhu, "Robust object-based multipass InSAR deformation reconstruction," *IIEEE Trans. Geosci. Remote Sens.*, vol. 55, no. 8, pp. 4239–4251, Aug. 2017.

[27] J.-S. Lee and E. Pottier, *Polarimetric Radar Imaging: From Basics to Applications*. Boca Raton, FL, USA: CRC Press, 2009.

[28] Y. Huang, L. Ferro-Famil, and A. Reigber, "Under-foliage object imaging using SAR tomography and polarimetric spectral estimators," *IEEE Trans. Geosci. Remote Sens.*, vol. 50, no. 6, pp. 2213–2225, Jun. 2012.

[29] E. Ferrara and T. Parks, "Direction finding with an array of antennas having diverse polarizations," *IEEE Trans. Antennas Propag.*, vol. AP-31, no. 2, pp. 231–236, Mar. 1983.
[30] M. L. Williams, "A coherent, polarimetric sar simulation of forests for PolSARPro," Tech. Rep., Oct. 12, 2015. [Online]. Available:https:// earth. eo. esa. int/polsarpro/Manuals/PolSARproSim_Design. pdf

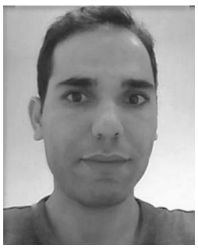

Hossein Aghababaee received the M.Sc. degree in remote sensing from the University of Tehran, Tehran, Iran, in 2012, and the Ph.D. degree in synthetic aperture radar remote sensing from the K. N. Toosi University of Technology, Tehran, Iran, in 2017.

In 2017, he joined the Telecommunication Group, University of Naples "Parthenope," Napoli, Italy, as a Research Fellow, after a visiting research period from November 2016 to May 2017. His research interests include SAR tomographic, target scattering decomposition, and polarimetric SAR processing for multidimensional geophysical information extraction.

Giampaolo Ferraioli (SM'17) was born in Lagonegro, Italy, in 1982. He received the B.S., M.S., and Ph.D. degrees in telecommunication engineering from the Universitá degli Studi di Napoli Parthenope, Naples, Italy, in 2003, 2005, and 2008, respectively.

He was a visiting scientist with Département TSI, Télécom ParisTech, Paris, France. He is currently an Assistant Professor with Universitá degli Studi di Napoli Parthenope. His main research interests include statistical signal and image processing, radar systems, synthetic aperture radar interferometry, and magnetic resonance imaging.

Dr. Ferraioli is an Associate Editor for the *Geoscience and Remote Sensing Letters*. He is member of the Technical Liaison Committee for the IEEE TRANSACTIONS ON COMPUTATIONAL IMAGING. In 2009, he was the recipient of the "IEEE 2009 Best European Ph.D. Thesis in Remote Sensing" prize, sponsored by IEEE Geoscience and Remote Sensing Society.

Gilda Schirinzi (M'14–SM'17) received the M.Sc. degree in electronic engineering from the University of Naples Federico II, Napoli, Italy, in 1983.

She joined the Department of Electronic Engineering, University of Naples Federico II, as a Research Fellow. From 1985 to 1986, she was with an European Space Agency, ESTEC, The Netherlands. In 1988, she joined the Istituto di Ricerca per l'Elettromagnetismo e i Componenti Elettronici (IRECE), Italian National Council of Researches, Napoli, Italy. In 1992, she was the Head of the Electromagnetics Division, IRECE. In 1997, she was a Senior Researcher. In 1998, she joined the University of Cassino, Cassino, Italy, as an Associate Professor of telecommunications. In 2005, she was a Full Professor. Since 2008, she has been with the Telecommunication Group, University of Naples "Parthenope," Napoli, Italy.

She has taught signal theory, electrical communications, microwave remote sensing systems, and image processing. Her research interests include SAR signal processing and coding, SAR interferometry and tomography, microwave imaging techniques, and image and signal processing for remote sensing applications.

Vito Pascazio (SM'11) received graduation degree (*summa cum laude*) in electronic engineering from the Universitá di Bari, Bari, Italy, in 1986, and the Ph.D. degree in electronic engineering and computer science from the Department of Electronic Engineering, Universitá di Napoli Federico II, Napoli, Italy.

In 1990, he was with the Research Institute on Electromagnetics and Electronic Devices, Italian National Council of Research, Napoli, Italy. He is currently a Full Professor and a Chair with the Department of Engineering, Universita di Napoli Parthenope, Napoli, Italy. From 1994 to 1995, he was a visiting scientist with the Laboratoire des Signaux et Systemes, Ecole Superieure d. Electricite (Supelec), Gif sur Yvette, France, and from 1998 to 1999, with the Universite de Nice Sophia-Antipolis, Nice, France. He is also the Director of National Laboratory of Multi-Media Communications of the Italian Consortium of Telecommunications, Napoli, Italy. He authored or coauthored more than 170 technical papers. His research interests include fields of remote sensing, and linear and non-linear estimation, with particular emphasis to image computing and processing, and reconstruction of microwave and radar images.

Dr. Pascazio was the recipient of the Philip Morris Prize for Scientific and Technological Research, in 1990. He was the General Co-Chairman of the IEEE Geoscience and Remote Sensing Society 2015 conference.